Letter

Low Overpotential Water Splitting Using Cobalt-Cobalt Phosphide (Co/CoP) Nanoparticles Supported on Nickel Foam

Justus Masa, Stefan Barwe, Corina Andronescu, Ilya Sinev, Adrian Ruff, Kolleboyina Jayaramulu, Karina Elumeeva, Bharathi Konkena, Beatriz Roldan Cuenya, and Wolfgang Schuhmann

ACS Energy Lett., **Just Accepted Manuscript** • DOI: 10.1021/acsenergylett.6b00532 • Publication Date (Web): 07 Nov 2016

ACS Energy Letters is published by the American Chemical Society. 1155 Sixteenth Street N.W., Washington, DC 20036

Low Overpotential Water Splitting Using Cobalt-Cobalt Phosphide (Co/Co_2P) Nanoparticles Supported on Nickel Foam

Justus Masa[†], Stefan Barwe[†], Corina Andronescu[‡†], Ilya Sinev[§], Adrian Ruff[†], Kolleboyina Jayaramulu[∓], Karina Elumeeva[†], Bharathi Konkena[†], Beatriz Roldan Cuenya[§], Wolfgang Schuhmann[†]**

† Analytical Chemistry - Center for Electrochemical Sciences (CES), Ruhr-Universität Bochum, Universitätsstr. 150, D-44780 Bochum (Germany)

‡ Department of Bioresources and Polymer Science, Faculty of Applied Chemistry and Materials Science, University "POLITEHNICA" Bucharest (Romania)

§ Department of Physics, Ruhr-Universität Bochum, Universitätsstr. 150, D-44780 Bochum (Germany)

∓ Chair II of Inorganic Chemistry, Ruhr-University Bochum, University Str. 150, 44801, Bochum

AUTHOR INFORMATION

***Corresponding Author**

justus.masa@rub.de

wolfgang.schuhmann@rub.de

ABSTRACT

We report a simple, facile and safe route for preparation of Co-Co phosphide (Co/Co_2P) nanoparticles and demonstrate their application as efficient low cost catalysts for electrochemical water splitting. The catalyst achieves good performance in catalyzing both the cathode and anode half-cell water splitting reactions in 1.0 M KOH, and the HER in an acidic electrolyte, 0.5 M H_2SO_4. For the OER in 1.0 M KOH, a current of 10 mA cm^{-2} was attained at 0.39 V overpotential on a glassy carbon electrode, while an overpotential of 0.19 V was attained at 50 mA cm^{-2} when the catalyst was supported on nickel foam.

TOC GRAPHIC

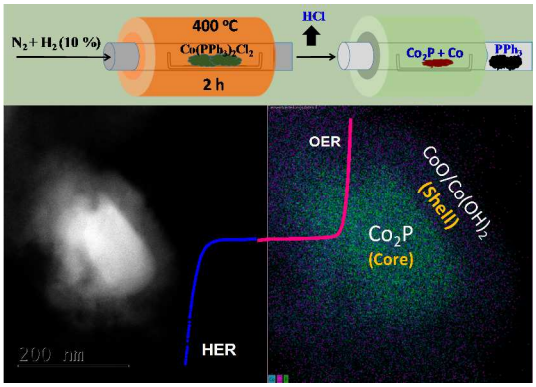

The conversion of electrical energy into portable gaseous or liquid fuels and chemicals, for example, by electrochemical water splitting to generate hydrogen and oxygen, is one of the most promising practical means to store energy from sources with intermittent intensity.[1,2] However, the production of viable quantities of hydrogen at a meaningful rate through the electrolysis of water is extremely energy intensive mostly stemming from the high overpotential required to drive the oxygen evolution reaction (OER) at the anode.[3] Moreover, the present state of the art catalysts for electrochemical water splitting, principally platinum group metals,[4] are not only rare but also overly costly. Research efforts continue to unravel ever more promising low cost, non-platinum group catalysts for electrochemical water splitting, mostly derived from earth abundant transition metals, typically Co, Fe, Mn and Ni based oxides or hydroxides for the OER,[5,6] and binary or ternary compositions of Co, Fe, Mn, Mo, W, and Ni with non-metals, typically, (C, N, S, P, Se, B, etc, for both the hydrogen evolution reaction (HER) and OER.[7–10] There are clear indications that the presence of non-metal and metalloid inclusions alters the surface electronic structure of the host metals and metal oxide or oxyhydroxides, leading to significant enhancement of their electrocatalytic ability, although the effects have not been exhaustively understood.[11,12] Metal phosphides are particularly interesting since they are highly active in electrocatalyzing both the OER and the HER.[8,12–14] However, the synthesis of metal phosphides presents challenges, particularly due to the fire hazardous nature of elemental phosphorous and some of its compounds.[12,15] Owing to the growing importance of metal phosphides in electrocatalysis, the development of simple, safe and scalable methods for their synthesis is extremely important.

We present a simple and safe method for the synthesis of cobalt-cobalt phosphide (Co/Co_2P) nanoparticles by thermal decomposition of dichloro(triphenylphosphine) cobalt ($(PPh_3)_2CoCl_2$)

under reductive conditions, and demonstrate their application as effective anode and cathode electrocatalysts for electrochemical water splitting under alkaline conditions, as well as very promising electrocatalysts for the HER under acidic conditions. When supported on nickel foam, the catalyst attains 50 mA cm^{-2} during OER at only 0.19 V overpotential, which is remarkable for a cobalt-based catalyst.

A scheme depicting the synthesis of the Co/Co_2P nanoparticles is shown in Figure 1a. Thermal gravimetric analysis (Fig. S1) revealed that $Co(PPh_3)_2Cl_2$ begins to decompose at about 180 ^oC, losing 80.5 % of its weight at 263 ^oC to form cobalt and cobalt phosphide nanoparticles, which were retained in the quartz boat, and a volatile white by-product (triphenylphosphine, PPh_3) which condensed right outside the heated zone of the CVD reactor. The identity of PPh_3 was confirmed by MS (m/z at 262 ($[M]^+$;100%); Fig.S2)) and NMR (^1H, ^{13}C and ^{31}P) analysis (Figures S3, S4 and S5). PPh_3 was recovered in pure form and can thus be used for further synthesis of $Co(PPh_3)_2Cl_2$ by its treatment with cobalt (II) chloride in alcohols or glacial acetic acid. Elemental analysis revealed that the product contained Co and P (Fig. 1b), with adventitious C and O (Fig. 2b). Carbon is expected to arise from Co catalyzed thermal degradation of the organic moieties of $Co(PPh_3)_2Cl_2$ while O is due to exposure of the product to air. The SEM micrograph in Figure 1b shows the microstructure of Co/Co_2P with the elemental composition in the overlaid EDX spectrum. Elemental EDX mapping reveals spatial overlap of the intensities of Co and P (Fig.1c-e) as would be expected of cobalt phosphide. XRD analysis of the product (Fig. 2a), revealed reflections which could be indexed to Co_2P (ICCD ref: 03-065-2380) as well as metallic cobalt (ICDD: 00-001-1255), indicating that the product comprised of Co_2P and Co nanoparticles. The equation

$$(PPh_3)_2CoCl_2 \rightarrow PPh_3 + Co/Co_2P + 2HCl_{(g)}$$

is proposed to represent the thermal decomposition of $(PPh_3)_2CoCl_2$ under synthesis conditions.

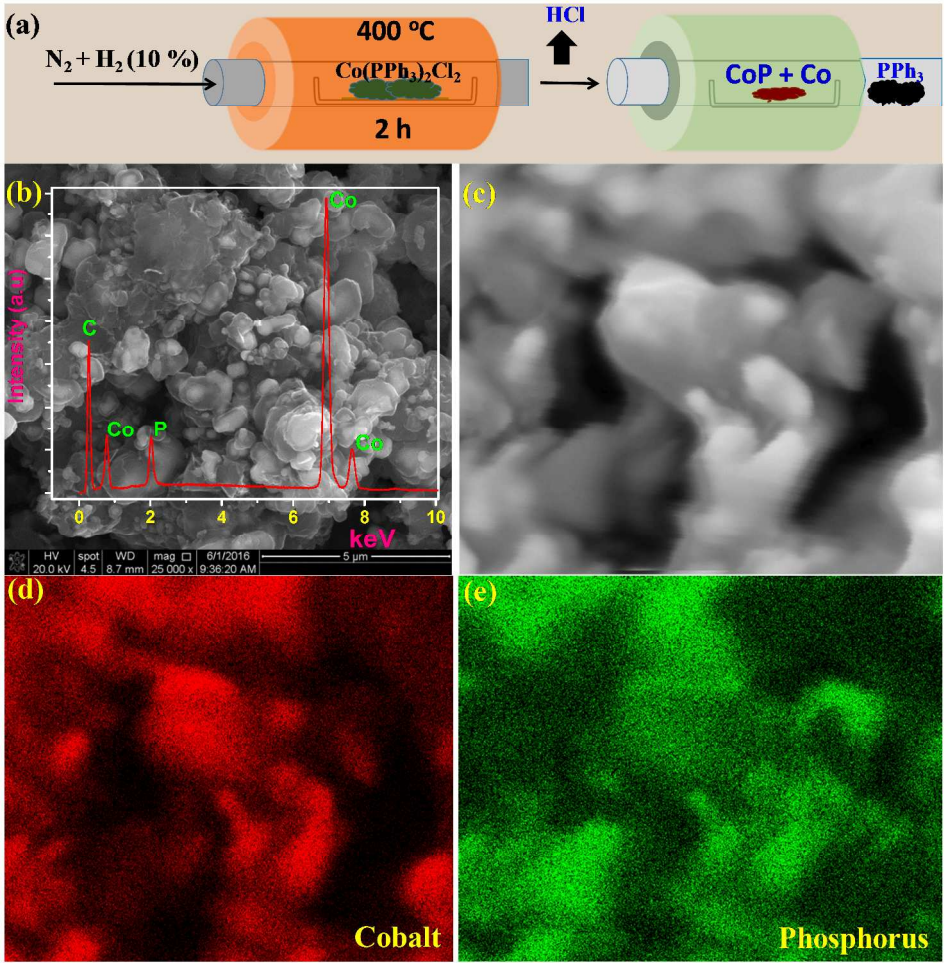

Figure 1. (a) Schematic representation of the synthesis of Co/Co_2P by thermal decomposition of $Co(PPh_3)_2Cl_2$ under reductive conditions, (b) representative SEM image of Co/Co_2P with an overlaid EDX spectrum, (c) region used for elemental mapping of Co (d) and P (e).

The chemical state of cobalt, phosphorus and oxygen in Co/Co_2P was probed by XPS to get insight in the structure-function correlation of the catalyst. The main peak of the Co $2p_{3/2}$ region is at 778 eV, similar to elemental cobalt and metal phosphides (Co_2P and CoP).[16,17] The $I_{satellite}$:$I_{core\text{-}line}$ ratio is 2.3, which perfectly fits to Co_2P,[16] consistent with the XRD results. The P 2p core level region was deconvoluted by two doublets, a sharp one with P $2p_{3/2}$ at 130.0 eV and

less intense and broad one with P 2p3/2 at 132.8 eV. The former matches both Co_2P and CoP within error of energy calibration,[16,18] while the latter can be ascribed to triphenylphosphine.[19] The presence of PPh_3 in the fresh sample is also obvious from the C 1s spectrum, where a distinctive $\pi \rightarrow \pi^*$ transition, typical of sp^2 hybridized organic molecules is observed (Figure S6). The synthesis yielded nanoparticles of cobalt, cobalt phosphide and trace triphenylphosphine.

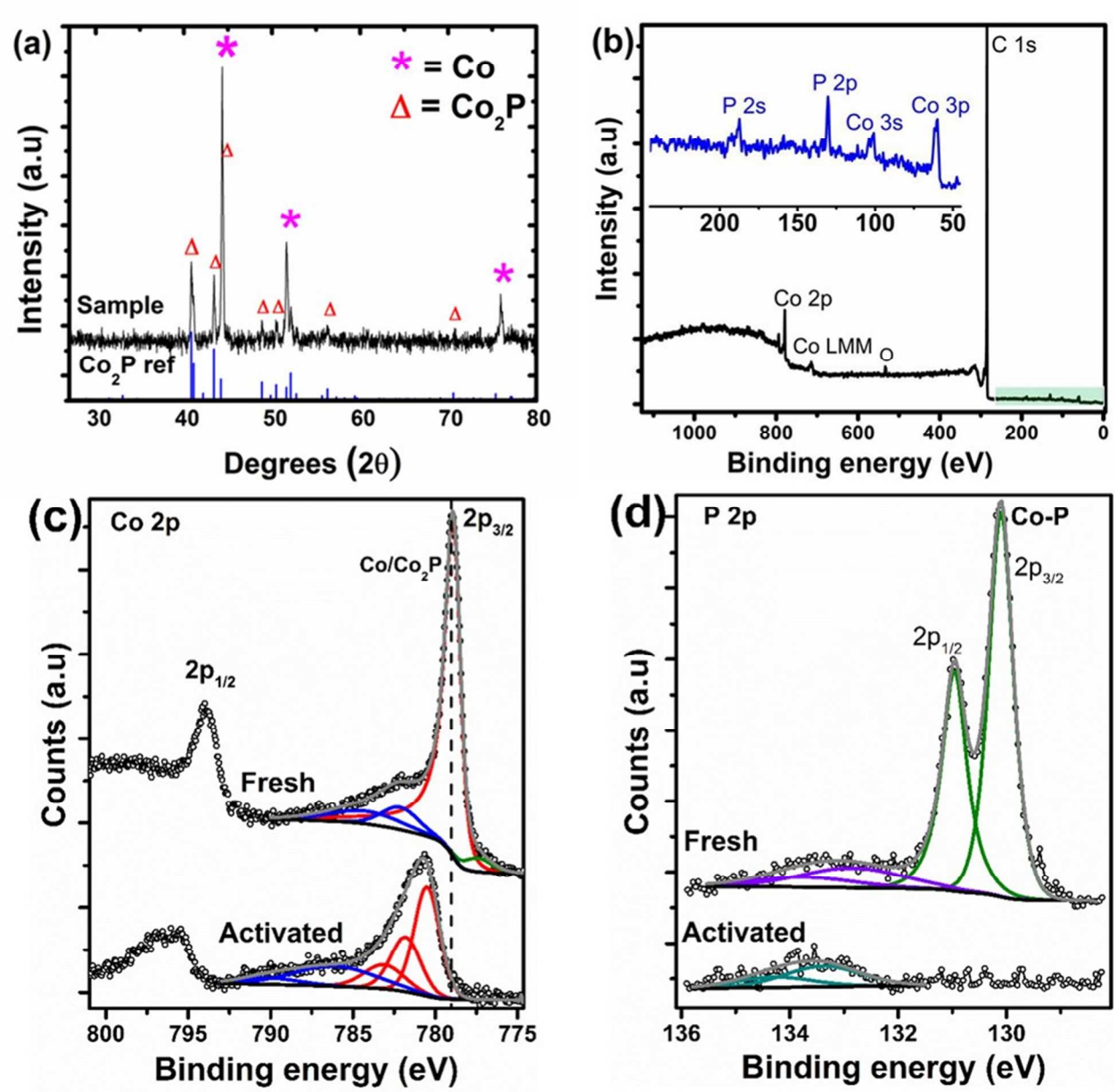

Figure 2. (a) X-ray diffraction pattern of Co/Co_2P, (b) XPS survey spectrum of Co/Co_2P with the inset showing an enlarged view of the phosphorus region, (c) high resolution Co 2p core level spectrum of Co/Co_2P before (fresh) and after electrochemical activation (activated), (d) high resolution P 2p core level spectra of Co/Co_2P before and after electrochemical activation.

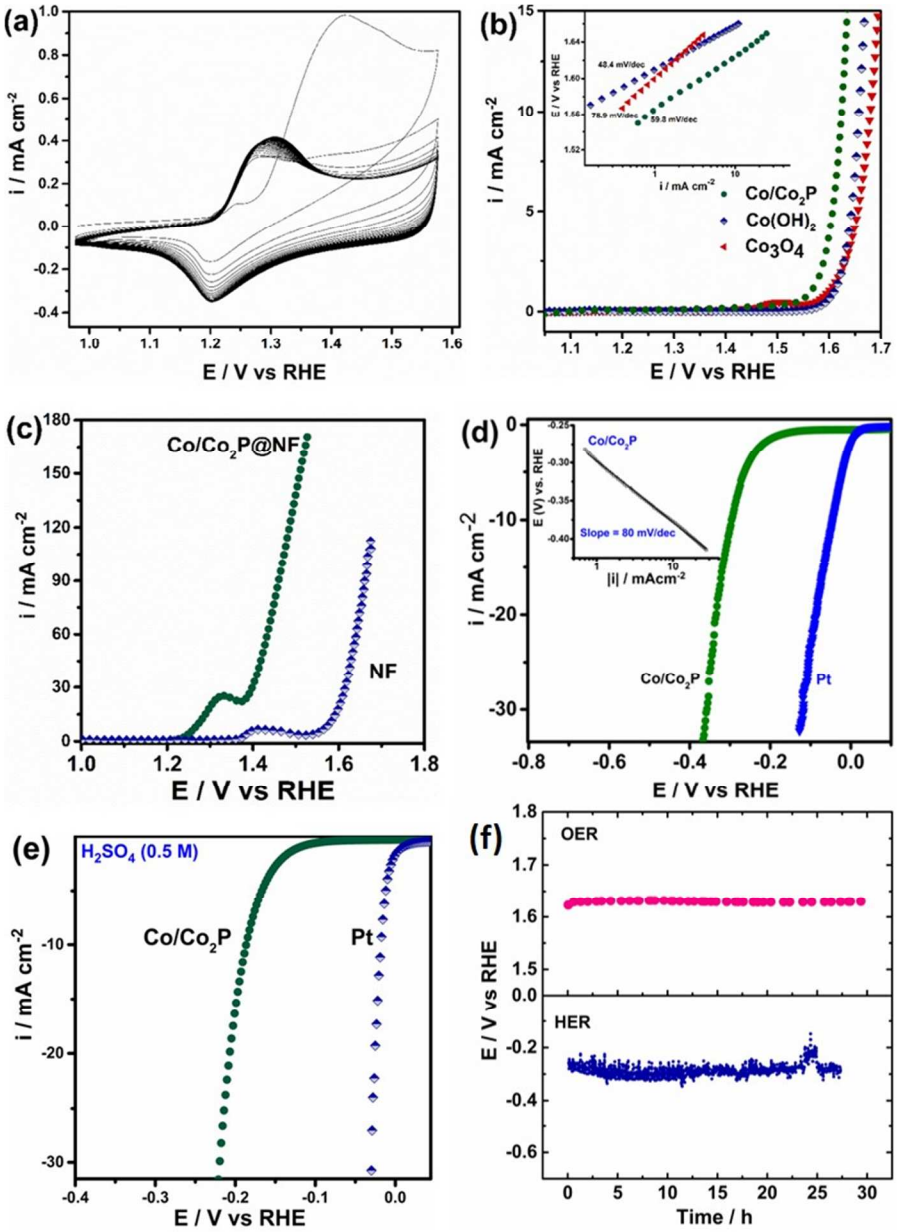

Figure 3. (a) Activation of Co/Co_2P by continuous potential cycling between 1.0 V and 1.58 V at 100 mV s^{-1} in 1.0 M KOH. (b) Linear sweep voltammograms (LSVs) of Co/Co_2P in 1.0 M

KOH juxtaposed with electrodeposited $Co(OH)_2$ and Co_3O_4, recorded under similar conditions; Inset is showing the corresponding afel plot. (c) LSVs showing the OER activity of Co/Co_2P supported on nickel foam (NF) (Co/Co_2P@NF) by drop coating compared with the OER activity of pure NF, (d) LSVs showing the HER activity of Co/Co_2P and Pt in 1.0 M KOH (inset is showing the corresponding Tafel plot) and (e) in 0.5 M H_2SO_4. (f) Chronopotentiometric curves showing the stability of Co/Co_2P supported on glassy carbon during OER and HER at a current density of 10 mA cm^{-2}. All the LSVs were recorded at a scan rate of 5 mV s^{-1} with electrode rotation at 1600 rpm to prevent the accumulation of gas bubbles.

The surface ratio of P:Co decreased from 0.75 in the non-activated sample to 0.15 in the electrochemically activated sample, and the dominant P $2p_{3/2}$ peak initially at 130.1 eV completely vanished. Only the broad less intense doublet with P $2p_{3/2}$ at 133.3 eV (Fig. 2d) characteristic of phosphates and pyrophosphates was observed. The OER principally takes place on a surface oxide/hydroxide layer, which for metallic species is formed prior to oxygen evolution, as demonstrated in Fig. 3a. HRTEM analysis of a Ni_2P OER catalyst after electrochemical pretreatment disclosed a core-shell (Ni_2P/NiO_x) structure, where phosphorus was concentrated in the core and oxygen was concentrated on the surface.[13] In the present study, not only cobalt but also surface P was oxidized under OER conditions. These observations support the prevalence of a core-shell (Co/Co_2P@CoO_x)–type structure proposed previously for metallic phosphides under OER conditions.[6,8,13,20] In this configuration, the metal oxide/hydroxide layer is the active electrocatalytic layer for the OER while the metal phosphide core is believed to act as a reservoir to stabilize reaction intermediates and as an electron conduit to promote facile charge transfer.

The electrochemical performance of Co/Co_2P towards water splitting, both OER and HER, was evaluated in 1.0 M KOH. Before collecting any data, the electrode was first subjected to continuous potential cycling in the potential window of interest until reproducible voltammograms were obtained. Figure 3a shows the evolution of the surface properties of Co/Co_2P with potential cycling at 100 mV s^{-1}. The sample undergoes irreversible oxidation during the first anodic scan due to formation of a surface oxide, followed by a gradual increase of the oxide film in the subsequent scans as manifested by the progressive increase of the anodic and cathodic peak currents at about 1.3 V and 1.2 V, respectively, ascribed to the redox reaction $CoO + OH^- \leftrightarrow CoOOH + e^-$.[21]

In a previous study, a lower intensity of the redox peaks after the first cycle was attributed to loss of the catalyst from the electrode, which was observed by means of a quartz crystal microbalance.[22] In principle, catalyst loss by physical detachment should be accompanied by decrease of the capacitive current. However, we observe the opposite effect, which further confirms that catalyst detachment does not suffice to account for the drop in intensity of the metal oxidation wave after the first cycle. Whereas we cannot completely rule out the likelihood that a similar scenario may partly account for the diminishment in the intensity of the oxidation peak after the first scan cycle, the fact that the intensities of both the oxidation and reduction waves continue to grow steadily from the second cycle onwards clearly supports the progressive growth of an oxide/hydroxide layer.

The activity of Co/Co_2P towards OER is shown in Figure 3b in the form of linear sweep voltammograms (LSV), corrected for the electrolyte resistance, along with results for Co_3O_4 (Sigma-Aldrich) electrodeposited cobalt hydroxide ($Co(OH)_2$) for the purpose of comparison. Co/Co_2P attained a current density of 10 mA cm^{-2} at 1.62 V vs. RHE, lower than $Co(OH)_2$ and

Co_3O_4 which attained the same current at 1.66 and 1.68 V vs. RHE, respectively (for further comparison see figure S7). This performance is comparable to recently reported performance of binary and ternary cobalt based catalysts incorporating a metalloid element or non-metal.[20] Nickel foam is increasingly used as a 3D-catalyst support owing to its high surface area and complimentary catalysis, leading to very high current densities at low overpotentials.[23,24] Co/Co_2P achieved 50 mA cm^{-2} at 1.42 V vs. RHE when supported on nickel foam (Fig. 3c). This performance matches that of state-of-the art nickel and cobalt based catalysts directly grown or supported on nickel foam.[24,25] A recent study by Dong et al.,[25] reported a binary Ni-Fe sulphide catalyst supported on nickel foam where a current density of 100 mA cm^{-2} was achieved at only 0.189 V overpotential. Meanwhile, Li and Zhao,[23] reported an iron doped nickel phosphate catalyst supported on nickel foam which achieved 500 mA cm^{-2} at an overpotential of 0.290 V in 1.0 M KOH. A detailed comparison of the performance of Co/Co_2P in relation to state-of the art OER catalysts is presented in table S1.

The outstanding performance of Co/Co_2P when supported on nickel foam warrants in-detail discussion. As can be seen from Fig. 3a, the oxidation of cobalt, $Co^{2+} \rightarrow Co^{3+/4+}$ commences at about 1.2 V with a peak at about 1.3 V, earlier than the oxidation of nickel, $Ni^{2+} \rightarrow Ni^{3+/4+}$ which has a peak between 1.4 and 1.5 V (Fig. 3c). When Co/Co_2P was supported on nickel foam (Fig. 3c), the potential for Co^{2+} to $Co^{3+/4+}$ oxidation was essentially similar to that on glassy carbon. However, the $Ni^{2+} \rightarrow Ni^{3+}$ oxidation wave which is obvious on bare nickel foam (Fig. 3c) is indiscernible on Co/Co_2P@NF. On the one hand, this indicates that nickel foam was almost fully covered by Co/Co_2P thus preventing the observation of the $Ni^{2+} \rightarrow Ni^{3+}$ fingerprint. On the other hand, synergistic interaction between two cations in metal hydroxides has been observed to cause a substantial shift on the potential for oxidation of the cations.[22,26] In a systematic study by

Enman et al.,[27] on the role of externally added cations on the OER activity of nickel (oxy)hydroxide, it was observed that some cations shift the Ni^{2+}/Ni^{3+} peaks to higher potentials while others shift them to lower potentials, although no direct correlation was found between the Ni^{2+}/Ni^{3+} redox potential and the measured OER activity. From Fig. 3c, it is therefore reasonable to conclude that the wave for $Ni^{2+} \rightarrow Ni^{3+}$ oxidation is merged with that for $Co^{2+} \rightarrow Co^{3+}/Co^{4+}$ oxidation, and with that for oxygen evolution. In addition to the high surface area of nickel foam, which we attribute to be primarily responsible for the enormous increase in the activity of Co/Co_2P@NF to high catalyst dispersion and enhanced mass transport through the porous network, synergetic interaction of activated Co/Co_2P and nickel can also contribute to activity enhancement. To illuminate on this supposition, we compared the OER activity of Co/Co_2P supported on a glassy carbon RDE electrode, and on a bulk nickel RDE electrode (Fig. S8). By employing Ni as the support, the potential at a current density of 10 mA cm^{-2} decreased from 1.62 V to 1.59 V, indicating clear existence of a synergetic effect. Activity enhancement of transition metal based OER catalysts can potentially accrue from the presence of Fe impurities, either in the electrolyte or in the catalyst.[22,26] In this study, Fe impurities, if any, did not pronouncedly affect the OER activity of Co/Co_2P@NF. If this was not the case, we would expect the OER activity of Ni-foam alone to be comparable to that of Co/Co_2P@NF.

The turn-over frequency (TOF) of O_2 evolution by Co/Co_2P and Co_3O_4 was determined to evaluate whether the presence of P imparts a unique effect on the electrocatalytic behavior of Co/Co_2P in contrast to its $Co(OH)_2$ and Co_3O_4 counter parts. The TOF at 1.65 V was 0.11 s^{-1} and 0.04 s^{-1}, respectively, for Co/Co_2P and CO_3O_4, calculated using the equation: TOF = i(A)/4eN, where N is the estimated number of atoms that participate in the reaction, e the electronic charge and i the current, and assuming that all the atoms loaded on the electrode participate in the

reaction. The obtained TOF of Co_3O_4 compares very well to reports of the TOF of cobalt based catalysts for OER, for example, Co_3O_4 (0.08 s^{-1}), Co (0.04 s^{-1}), and CoO (0.04 s^{-1}) nanoparticles, and related cobalt and nickel catalysts.[28–30] The results thus indicate that each active site of Co/Co_2P is potently more active than that of Co_3O_4 evaluated under similar conditions. Since TOF is an intensive catalytic parameter, independent of surface area effects, one would expect the TOF of Co/CoP, Co_3O_4 and electrodeposited $Co(OH)_2$ to be within a similar range if phosphorus only played a passive role in Co/Co_2P. The fact that the TOF of Co/Co_2P is substantially higher than for $Co(OH)_2$ and Co_3O_4 strongly suggests that P most likely plays a crucial role in promoting the OER activity of Co/Co_2P. Evidently, the interaction of P with Co is expected to alter the surface electronic structure of Co and thus its surface reactivity.[31] The Tafel slope of Co/Co_2P during OER (Figure 3b inset) was 59.8 mV/dec, substantially lower than that for Co_3O_4 (78.9 mV/dec), and fits well to the theoretical value of $2.303RT/\alpha F$ (where F is the Faraday constant, T is the absolute temperature, R is the universal gas constant and α is transfer coefficient), ascribed to the first electron transfer step being limiting.[32] By contrast, both chemical and electron transfer steps are apparently decisive on the kinetics of the OER on Co_3O_4, the Tafel slope of the OER on $Co(OH)_2$, 48.4 mV/dec, indicating that the first electron transfer step on this catalyst is kinetically faster than on Co/Co_2P. However, the fact that the overpotential of the OER was comparatively lower on Co/Co_2P compared to $Co(OH)_2$, implies that the overall kinetics of the OER was faster on the former. The Faradaic efficiency of the Co/Co_2P catalyst for the OER was determined by means of RRDE measurements to be 98.9±3.8 % (for detailed information see the SI).

To shed further light on the state of the catalyst under OER reaction conditions, post-mortem analysis of a film of the catalyst deposited on a clean piece of carbon paper and subjected to

electrochemical conditioning (50 CVs between 1.0 and 1.65 V), followed by polarization at 10 mA cm^{-2} for 300 s was analyzed by XPS. The features of the Co 2p region of the electrochemically activated sample (Fig. 2c) fit a Co_3O_4-like surface structure,[13] indicating that the surface of the catalyst was covered with oxide/hydroxide species after the electrochemical activation process.

Further post-mortem analysis of the catalyst was performed by transmission electron microscopy (TEM) with an integrated EDX detector. Figure 4 shows a representative scanning TEM (STEM) image of an electrochemically activated Co/Co_2P particle with corresponding EDX intensity maps showing the distribution of Co, P and O in the catalyst. A clear contrast of two morphologies on an individual particle can be seen in the STEM image in Fig. 4a. The EDX intensities maps of Co, P, and O show evidence of a core@shell ($Co_2P@CoO_x$) structure after electrochemical activation of Co/Co_2P, which contrasts the image before the activation (Fig. S9). The HRTEM image in Fig. 4b shows crystalline domains at the center and a less crystalline domain at the periphery. In addition, the atomic columns of the crystalline domain are depicted in Fig. 4c.

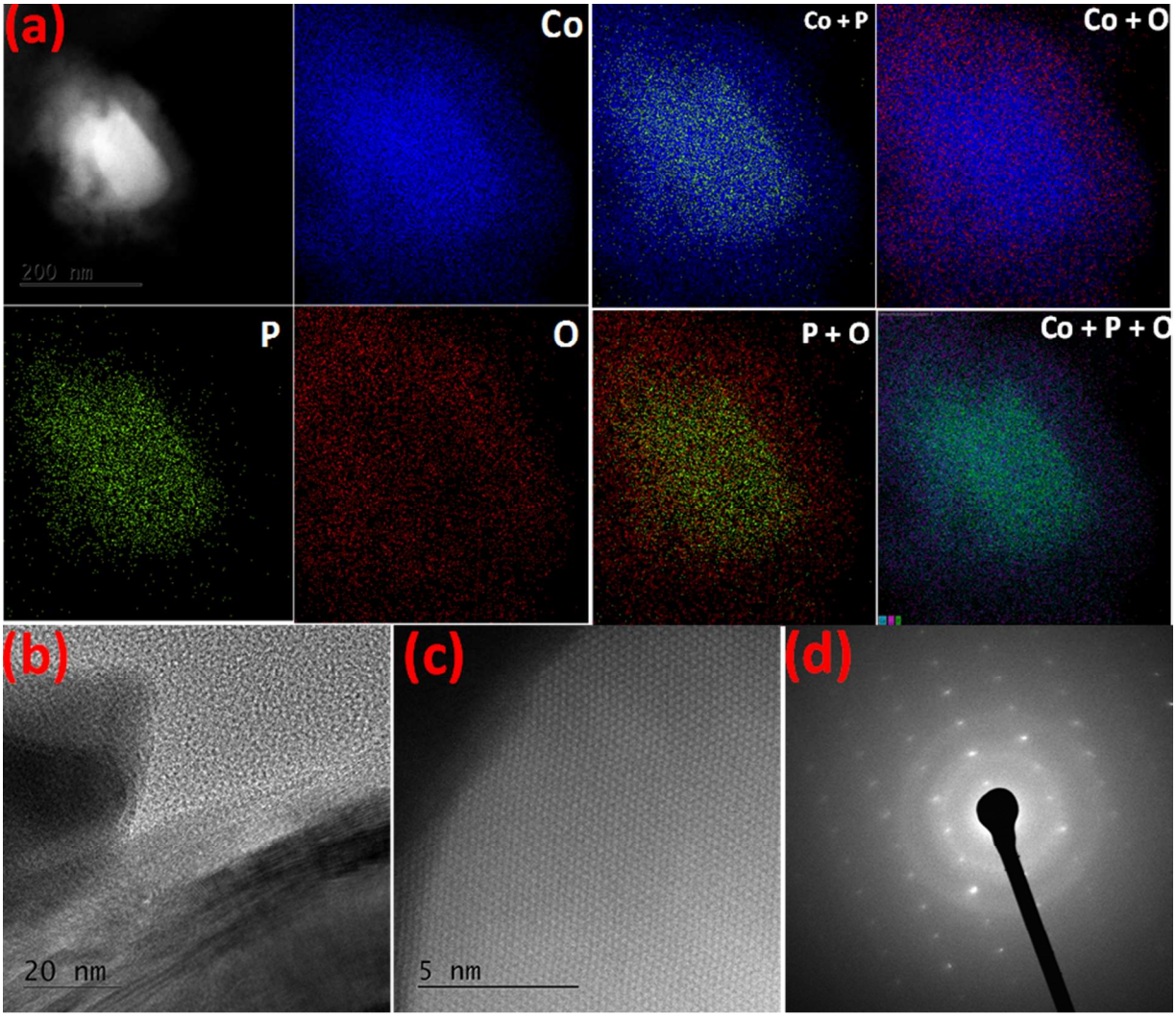

Figure 4. Post-mortem TEM analysis of electrochemically activated Co/Co_2P: (a) High resolution scanning transmission electron microscopy (STEM) image EDX intensity maps showing the distribution of Co, P and O (scale bar represents 200 nm), (b) HRTEM image of Co/Co_2P, (c) atomic scale HRTEM image taken from the crystalline domain at the center of a Co/Co_2P particle, (d) selected area electron diffraction (SAED) pattern taken from the center of a Co/Co_2P particle.

Selected area electron (SAED) disclosed that the core of the particles was highly crystalline (Fig. 4d), while the rim is less crystalline. Notably, the results show that phosphorus remains a

part of the activated catalyst. The bulk Co:P ratio determined by TEM/EDX in the activated catalyst was 1.69, essentially similar to that of the non-activated catalyst, with a Co:P ratio of 1.73 (see Fig. S10 and S11).

The potential of Co/Co_2P to catalyze the HER was investigated under both alkaline and acidic conditions and the results are presented in Figures 3d and 3e, respectively, and compared with Pt. Co/Co_2P attained a current density of 10 mA cm^{-2} at overpotentials of 0.295 V in KOH and 0.186 V in H_2SO_4, which are 0.150 V and 0.168 V higher than on Pt in the respective electrolytes. The Tafel slopes for the HER were 80 mV/dec for Co/Co_2P and 28.7 mV/dec for Pt in KOH, and 156 mV/dec for Co/Co_2P and 56.7 mV/dec for Pt in H_2SO_4. Thus, under alkaline conditions, the HER on Co/Co_2P appears to be controlled by a mixed Volmer-Heyrovsky mechanism, while the Volmer mechanism appears to be dominant under acidic conditions. In contrast, the HER on Pt was governed by the Tafel mechanism under alkaline conditions and mainly by the Heyrovsky mechanism under acidic conditions in agreement with the literature.[25]

The long-term performance of the catalyst was evaluated independently for the OER and HER in 1.0 M KOH at an absolute current density of 10 mA cm^{-2} (Fig. 3f). During the durability measurements, the electrode was maintained at a rotation speed of 1600 rpm to avoid the accumulation of gas bubbles on the electrode surface. The catalyst maintained a very stable performance for at least 30 h during both HER and OER without any indication of activity degradation.

In conclusion, a simple, safe and facile method for synthesis of cobalt phosphide nanoparticles, as low cost catalyst for electrochemical water splitting is reported. The synthesis involved reductive thermal treatment of dichloro(triphenylphosphine)cobalt $(PPh_3)_2CoCl_2$) in a N_2 atmosphere containing 10 % H_2. The developed material achieves excellent catalysis of water

splitting, at both the anode and cathode under alkaline conditions, as well as very promising electrocatalysis of the HER under acidic conditions. When supported on nickel foam, the catalyst achieves a current density of 50 mA cm^{-2} at overpotential of only 0.19 V during the OER, which is remarkable for a non-platinum group catalyst. Under OER conditions, the surface of the catalyst is oxidized to form a surface oxide/oxyhydroxide layer, which is the active layer upon which the OER proceeds. The catalyst sustained stable performance at a current of 10 mA cm^{-2} for at least 30 h, for both the cathode and anode half-cell reactions thus manifesting its potential to endure stable performance under practical conditions.

ASSOCIATED CONTENT

Supporting Information, including: materials and experimental methods, TGA, MS, NMR and XPS data.

AUTHOR INFORMATION

justus.masa@rub.de, wolfgang.schuhmann@rub.de, www.rub.de/elan

NOTES

The authors declare no competing financial interest.

ACKNOWLEDGMENT

The authors are grateful to the Deutsche Forschungsgemeinschaft (DFG) in the framework of the Cluster of Excellence Resolv (EXC1069) and the Bundesministerium für Bildung und Forschung (BMBF) in the frameworks of the project "Mangan" (FKZ 03EK3548)

REFERENCES

(1) Lewis, N. S.; Nocera, D. G. Powering the planet: Chemical challenges in solar energy utilization. *Proc. Natl. Acad. Sci. USA.* **2006**, *103*, 15729–15735.

(2) Schmidt, D. G. Research opportunities for future energy technologies. *ACS Energy Lett.* **2016**, *1*, 244–245.

(3) Zeng, K.; Zhang, D. Recent progress in alkaline water electrolysis for hydrogen production and applications. *Prog. Energ. Combust* **2010**, *36*, 307–326.

(4) McCrory, C. C. L.; Jung, S.; Ferrer, I. M.; Chatman, S. M.; Peters, J. C.; Jaramillo, T. F. Benchmarking hydrogen evolving reaction and oxygen evolving reaction electrocatalysts for solar water splitting devices. *J. Am. Chem. Soc.* **2015**, *137*, 4347–4357.

(5) Gao, M.-R.; Cao, X.; Gao, Q.; Xu, Y.-F.; Zheng, Y.-R.; Jiang, J.; Yu, S.-H. Nitrogen-doped graphene supported CoSe□ nanobelt composite catalyst for efficient water oxidation. *ACS nano* **2014**, *8*, 3970–3978.

(6) Ryu, J.; Jung, N.; Jang, J. H.; Kim, H.-J.; Yoo, S. J. In situ transformation of hydrogen-evolving CoP nanoparticles: Toward efficient oxygen evolution catalysts bearing dispersed morphologies with Co-oxo/hydroxo molecular units. *ACS Catal.* **2015**, *5*, 4066–4074.

(7) Xu, K.; Chen, P.; Li, X.; Tong, Y.; Ding, H.; Wu, X.; Chu, W.; Peng, Z.; Wu, C.; Xie, Y. Metallic nickel nitride nanosheets realizing enhanced electrochemical water oxidation. *J. Am. Chem. Soc.* **2015**, *137*, 4119–4125.

(8) Stern, L.-A.; Feng, L.; Song, F.; Hu, X. Ni_2P as a Janus catalyst for water splitting: The oxygen evolution activity of Ni_2P nanoparticles. *Energy Environ. Sci.* **2015**, *8*, 2347–2351.

(9) Masa, J.; Weide, P.; Peeters, D.; Sinev, I.; Xia, W.; Sun, Z.; Somsen, C.; Muhler, M.; Schuhmann, W. Amorphous cobalt boride (Co_2B) as a highly efficient nonprecious catalyst for electrochemical water splitting: oxygen and hydrogen evolution. *Adv. Energy Mater.* **2016**, 1502313.

(10) Popczun, E. J.; McKone, J. R.; Read, C. G.; Biacchi, A. J.; Wiltrout, A. M.; Lewis, N. S.; Schaak, R. E. Nanostructured nickel phosphide as an electrocatalyst for the hydrogen evolution reaction. *J. Am. Chem. Soc.* **2013**, *135*, 9267–9270.

(11) Chen, S.; Thind, S. S.; Chen, A. Nanostructured materials for water splitting - state of the art and future needs: A mini-review. *Electrochem. Commun* **2016**, *63*, 10–17.

(12) Read, C. G.; Callejas, J. F.; Holder, C. F.; Schaak, R. E. General strategy for the synthesis of transition metal phosphide films for electrocatalytic hydrogen and oxygen evolution. *ACS Appl. Mater. Interfaces* **2016**, *8*, 12798–1280

(13) Dutta, A.; Samantara, A. K.; Dutta, S. K.; Jena, B. K.; Pradhan, N. Surface-oxidized dicobalt phosphide nanoneedles as a nonprecious, durable, and efficient OER catalyst. *ACS Energy Lett.* **2016**, *1*, 169–174.

(14) Popczun, E. J.; Read, C. G.; Roske, C. W.; Lewis, N. S.; Schaak, R. E. Highly active electrocatalysis of the hydrogen evolution reaction by cobalt phosphide nanoparticles. *Angew. Chem. Int. Ed.* **2014**, *53*, 5427–5430.

(15) Brock, S. L.; Perera, S. C.; Stamm, K. L. Chemical routes for production of transition-metal phosphides on the nanoscale: implications for advanced magnetic and catalytic materials. *Chem. Eur. J.* **2004**, *10*, 3364–3371.

(16) Blanchard, P. E. R.; Grosvenor, A. P.; Cavell, R. G.; Mar, A. X-ray Photoelectron and absorption spectroscopy of metal-rich phosphides M_2P and M_3P (M = Cr−Ni). *Chem. Mater.* **2008**, *20*, 7081–7088.

(17) Biesinger, M. C.; Payne, B. P.; Grosvenor, A. P.; Lau, L. W.; Gerson, A. R.; Smart, R. S. Resolving surface chemical states in XPS analysis of first row transition metals, oxides and hydroxides: Cr, Mn, Fe, Co and Ni. *Appl. Surf. Sci* **2011**, *257*, 2717–2730.

(18) Okamoto, Y.; Nitta, Y.; Imanaka, T.; Teranishi, S. Surface characterisation of nickel boride and nickel phosphide catalysts by X-ray photoelectron spectroscopy. *J. Chem. Soc., Faraday Trans. 1* **1979**, *75*, 2027–2039.

(19) Yerushalmi, R.; Ho, J. C.; Fan, Z.; Javey, A. Phosphine oxide monolayers on SiO_2 surfaces. *Angew. Chem. Int. Ed.* **2008**, *120*, 4512–4514.

(20) Chang, J.; Xiao, Y.; Xiao, M.; Ge, J.; Liu, C.; Xing, W. Surface oxidized cobalt-phosphide nanorods as an advanced oxygen evolution catalyst in alkaline solution. *ACS Catal.* **2015**, *5*, 6874–6878.

(21) Risch, M.; Ringleb, F.; Kohlhoff, M.; Bogdanoff, P.; Chernev, P.; Zaharieva, I.; Dau, H. Water oxidation by amorphous cobalt-based oxides: In situ tracking of redox transitions and mode of catalysis. *Energy Environ. Sci.* **2015**, *8*, 661–674.

(22) Burke, M. S.; Kast, M. G.; Trotochaud, L.; Smith, A. M.; Boettcher, S. W. Cobalt-iron (oxy)hydroxide oxygen evolution electrocatalysts: the role of structure and composition on activity, stability, and mechanism. *J. Am. Chem. Soc.* **2015**, *137*, 3638–3648.

(23) Li, Y.; Zhao, C. Iron-doped nickel phosphate as synergistic electrocatalyst for water oxidation. *Chem. Mater.* **2016**, *28*, 5659–5666.

(24) Zhou, W.; Wu, X.-J.; Cao, X.; Huang, X.; Tan, C.; Tian, J.; Liu, H.; Wang, J.; Zhang, H. Ni_3S_2 nanorods/Ni foam composite electrode with low overpotential for electrocatalytic oxygen evolution. *Energy Environ. Sci.* **2013**, *6*, 2921–2924.

(25) Dong, B.; Zhao, X.; Han, G.-Q.; Li, X.; Shang, X.; Liu, Y.-R.; Hu, W.-H.; Chai, Y.-M.; Zhao, H.; Liu, C.-G. Two-step synthesis of binary Ni–Fe sulfides supported on nickel foam as highly efficient electrocatalysts for the oxygen evolution reaction. *J. Mater. Chem. A* **2016**, *4*, 13499–13508.

(26) Trotochaud, L.; Young, S. L.; Ranney, J. K.; Boettcher, S. W. Nickel-iron oxyhydroxide oxygen-evolution electrocatalysts: the role of intentional and incidental iron incorporation. *J. Am. Chem. Soc.* **2014**, *136*, 6744–6753.

(27) Enman, L. J.; Burke, M. S.; Batchellor, A. S.; Boettcher, S. W. Effects of intentionally incorporated metal cations on the oxygen evolution electrocatalytic activity of nickel (oxy)hydroxide in alkaline media. *ACS Catal.* **2016**, *6*, 2416–2423.

(28) Liu, Y.; Cheng, H.; Lyu, M.; Fan, S.; Liu, Q.; Zhang, W.; Zhi, Y.; Wang, C.; Xiao, C.; Wei, S.; Ye, B.; Xie, Y. Low overpotential in vacancy-rich ultrathin $CoSe_2$ nanosheets for water oxidation. *J. Am. Chem. Soc.* **2014**, *136*, 15670–15675.

(29) Yeo, B. S.; Bell, A. T. Enhanced activity of gold-supported cobalt oxide for the electrochemical evolution of oxygen. *J. Am. Chem. Soc.* **2011**, *133*, 5587–5593.

(30) Esswein, A. J.; McMurdo, M. J.; Ross, P. N.; Bell, A. T.; Tilley, T. D. Size-dependent activity of Co_3O_4 nanoparticle anodes for alkaline water electrolysis. *J. Phys. Chem. C* **2009**, *113*, 15068–15072.

(31) Burke, M. S.; Enman, L. J.; Batchellor, A. S.; Zou, S.; Boettcher, S. W. Oxygen evolution reaction electrocatalysis on transition metal oxides and (oxy)hydroxides: activity trends and design principles. *Chem. Mater.* **2015**, *27*, 7549–7558.

(32) Shinagawa, T.; Garcia-Esparza, A. T.; Takanabe, K. Insight on Tafel slopes from a microkinetic analysis of aqueous electrocatalysis for energy conversion. *Sci. Rep.* **2015**, *5*, 13801.